NEUROSCIENCE

Emilin 2 promotes the mechanical gradient of the cochlear basilar membrane and resolution of frequencies in sound

Ian J. Russell[1]*, Victoria A. Lukashkina[1], Snezana Levic[1,2], Young-Wook Cho[3], Andrei N. Lukashkin[1], Lily Ng[3], Douglas Forrest[3]*

The detection of different frequencies in sound is accomplished with remarkable precision by the basilar membrane (BM), an elastic, ribbon-like structure with graded stiffness along the cochlear spiral. Sound stimulates a wave of displacement along the BM with maximal magnitude at precise, frequency-specific locations to excite neural signals that carry frequency information to the brain. Perceptual frequency discrimination requires fine resolution of this frequency map, but little is known of the intrinsic molecular features that demarcate the place of response on the BM. To investigate the role of BM microarchitecture in frequency discrimination, we deleted extracellular matrix protein emilin 2, which disturbed the filamentous organization in the BM. *Emilin2*$^{-/-}$ mice displayed broadened mechanical and neural frequency tuning with multiple response peaks that are shifted to lower frequencies than normal. Thus, emilin 2 confers a stiffness gradient on the BM that is critical for accurate frequency resolution.

INTRODUCTION

The basilar membrane (BM), an elastic, ribbon-like structure in the mammalian cochlea, plays a central role in mediating the mechanical decomposition of sound into individual frequency components, a key feature of auditory function. The BM is graded along its length with respect to its dimensions (width and thickness) and stiffness, which forms the basis for a frequency-to-place (tonotopic) map (*1*). The apical, most compliant region of the BM is sensitive to lower frequencies, whereas the basal, stiffer region is sensitive to higher frequencies. G. von Békésy (*1*) found that excitation by sound pressure introduced at any point along the cochlea propagates a traveling wave from base to apex with peak amplitude at a frequency-specific location on the BM. This tonotopic cochlear frequency map is an organizing principle that enables neural encoding of frequency information.

Frequency analysis is fundamental to all auditory functions and begins when sound-induced vibration of the BM causes shear displacements of the stereociliary bundles of the mechanosensory hair cells that gate conductances in the stereociliary tips. Dynamic interactions between the BM, hair cells, and other structures of the organ of Corti transduce sounds into electrical signals that are relayed to the brain to elicit perception and behavior (*2*). Fine frequency resolution determines auditory perceptual abilities that underlie communication and learning, such as the ability to listen for, or discriminate between, sounds in complex acoustic environments (*3*).

Although the overall dimensions of the BM provide the anatomical framework for the frequency response map, little is known of constituent proteins that determine the mechanical gradient of the BM. The BM consists of an extracellular matrix in which radial collagenous filaments are interspersed in ground substance (*4*, *5*). These filaments contain collagen II and are thought to confer structural support and stiffness on the BM (*6*). The shape of the BM varies between species and may correlate with frequency resolution and range (*7*). The pectinate (lateral) zone of the BM in certain mammals with high-frequency hearing, including the mouse and some *Talpa* species (*8*), is more bulbous than that, for example, in humans. It has also been suggested in a modeling study in the gerbil that the proportion of filaments in the arcuate (medial) zone influences the frequency gradient of the BM (*9*). However, knowledge of the protein composition of the BM is limited, being based mainly on immunostaining (*10*, *11*) and functional analysis of specific components is lacking.

We previously identified *Emilin2* (elastin microfiber interfacer 2) as a defectively expressed cochlear gene in mice that lack a thyroid hormone receptor (*12*). Emilin family glycoproteins contribute to varied extracellular functions and tissue elasticity. Emilin 1 and emilin 2 can associate with microfibrils in skin extracts (*13*), and *Emilin1*-deficient mice display narrowing of blood vessels and hypertension (*14*). Emilin 2 has been reported to influence angiogenesis (*15*) and thrombosis (*16*), but its wider roles are unknown. The prominent expression of emilin 2 in the cochlea compared to other tissues (*12*) led us to investigate a specific role in frequency resolution. We report that emilin 2 is required to organize the filamentous architecture of the BM in mice. Mechanical and neural analyses indicate that emilin 2 confers critical stiffness on the BM and allows fine resolution of cochlear frequency tuning.

RESULTS

Expression pattern and deletion of *Emilin2* in the cochlea

The cellular expression of *Emilin2* was mapped in heterozygous mice carrying a *lacZ* reporter knock-in that replaced the first two coding exons of the gene (Fig. 1A). Homozygous *Emilin2*$^{-/-}$ mice lacked emilin 2 protein, as shown by Western blot analysis of cochlear tissue (Fig. 1B), and were subsequently used for loss-of-function studies. In immature *Emilin2*$^{+/-}$ mice, *lacZ* was expressed in the tympanic border cells on the underside of the BM along the basal-apical length of the cochlear spiral, as detected by histochemistry for the β-galactosidase

[1]Sensory Neuroscience Research Group, School of Pharmacy and Biomolecular Sciences, University of Brighton, Huxley Building, Brighton BN2 4GJ, UK. [2]Brighton and Sussex Medical School, University of Sussex, Brighton BN1 9PX, UK. [3]Laboratory of Endocrinology and Receptor Biology, NIDDK, National Institutes of Health, Bethesda, 10 Center Drive, MD 20892, USA.
*Corresponding author. Email: i.russell@brighton.ac.uk (I.J.R.); forrestd@niddk.nih.gov (D.F.)

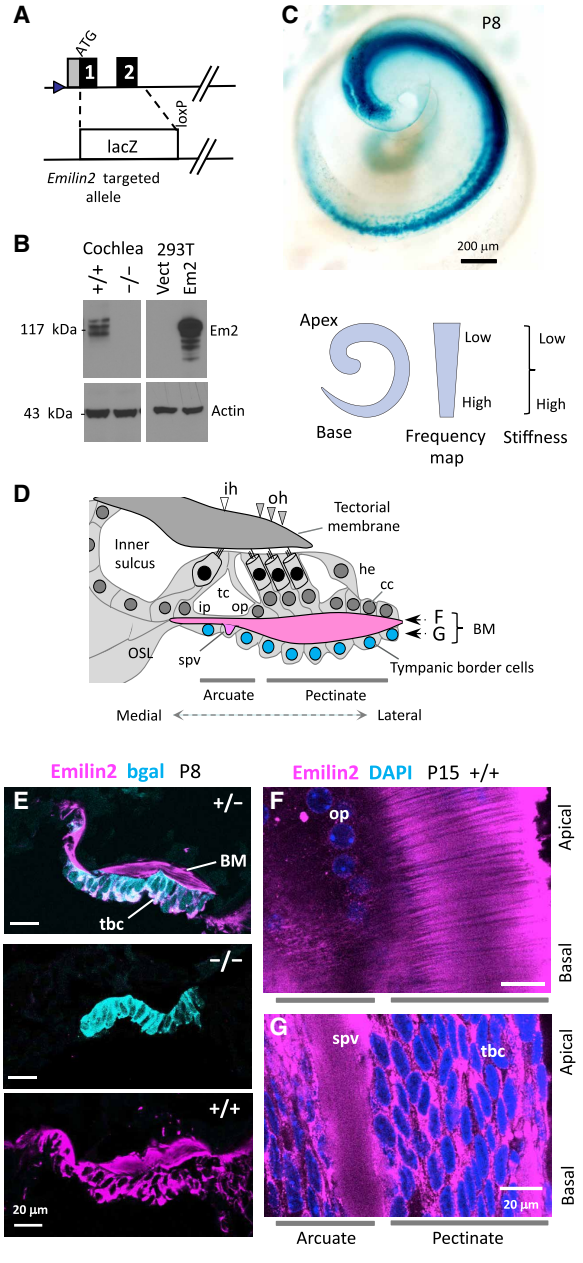

Fig. 1. *Emilin2* expression and deletion in the cochlea. (**A**) In the *Emlin2* reporter allele, *lacZ* replaces the first two coding exons of the gene. Gray box, 5′-untranslated region; arrowhead, promoter. (**B**) Western blot of cochlea (P8) from +/+ and Emilin2$^{-/-}$ mice and for control 293T cells transfected with *Emilin2* expression vector (Em2) or empty vector (vect). The blot was reprobed for actin, as control. (**C**) Histochemical detection of β-galactosidase [encoded by *lacZ* (blue)] in the BM in intact cochlea in an *Emilin2*$^{+/-}$ pup. BM spiral and "unwound" spiral diagrams depict gradients of width and frequency sensitivity along the BM. (**D**) Diagram of the organ of Corti. (**E**) Immunofluorescence analysis of emilin 2 protein (red) and β-galactosidase protein (blue) in cryosections of +/+, +/−, and −/− mice. Whitish color, double-positive cells in +/− mice. (**F** and **G**) In the organ of Corti flat mounts, emilin 2 (red) was in the acellular BM (F) and in tympanic border cell (tbc) and spiral vessel (spv) (G). Cell nuclei, blue [4′,6-diamidino-2-phenylindole (DAPI)]. cc, Claudius cells; he, Hensen cells; ih, inner hair cell; ip, inner pillar cell; oh, outer hair cell; op, outer pillar cell; OSL, osseous spiral lamina; SL, spiral ligament; tc, tunnel of Corti.

product (Fig. 1C). Expression was detected in tympanic border cells in both the arcuate and pectinate zones of the BM, in accord with in situ hybridization data (*12*). The arcuate zone spans between the feet of the inner and outer pillar cells, whereas the pectinate zone extends from the outer pillar cell to the lateral wall of the cochlea (Fig. 1D).

Immunofluorescence analysis on cochlear sections of wild-type (+/+) and *Emilin2*$^{+/-}$ mice detected endogenous emilin 2 protein in both the tympanic border cells and extracellular matrix of the BM, consistent with the tympanic border cells being the source of emilin 2 that is secreted into the BM (Fig. 1E). The protein was undetected in *Emilin2*$^{-/-}$ mice, confirming the ablation of the gene. Analysis of flat mounts of the organ of Corti from +/+ or +/− mice (Fig. 1, F and G) similarly detected emilin 2 in the BM and tympanic border cells. The flat mounts also indicated the radial filamentous structure of the BM, revealed in relief since emilin 2 immunoreactivity localizes mainly in the ground substance matrix around the filaments (*12*). The collagenous filaments appear as radial bundles in the pectinate zone and as looser fibers in the arcuate zone.

Developmentally, *lacZ* expression began in newborns and then peaked ~2 weeks later during the maturation of the organ of Corti and onset of hearing in juvenile mice (fig. S1). Expression of *lacZ* declined in adults and became restricted to apical regions because of the progressive loss of tympanic border cells in middle and basal regions. However, emilin 2 protein persisted in the acellular matrix in all cochlear turns in adults, indicating that the secreted protein is a stable constituent of the BM (fig. S1).

Disarray of BM architecture in *Emilin2*$^{-/-}$ mice

The localization of emilin 2 primarily in the ground substance of the acellular BM (*12*) led us to test whether emilin 2 organizes the microarchitecture within the BM. In adult *Emilin2*$^{-/-}$ mice, the organ of Corti was intact without obvious degeneration or loss of hair cells (Fig. 2A), but the acellular BM was slightly compacted (cross-sectional area of the pectinate zone) relative to the width of the BM (medial to lateral) in histological sections (Fig. 2, B and C). The BM normally narrows, and the pectinate zone becomes thicker and more bulbous in the apical to basal direction. The subtle thinning of the BM in *Emilin2*$^{-/-}$ mice was consistent in apical, middle, and basal turns of the cochlea. The morphology of the organ of Corti, otherwise, had a normal histological appearance in all turns of the cochlea examined (fig. S2). The phenotype did not worsen at several months of age, indicating an absence of progressive degeneration.

Transmission electron microscopy of BM ultrastructure revealed a loss of ground substance relative to filamentous area in sections of the BM in *Emilin2*$^{-/-}$ mice (Fig. 2, D and E; mid-basal turns). In the pectinate zone, radial collagenous filament bundles are normally interspersed in ground substance, but in *Emilin2*$^{-/-}$ mice, dense filaments dominated the BM, suggesting that disordered collagenous fibers occupied space that is normally filled by ground substance. The filaments retained a general radial orientation. The results suggest that emilin 2 promotes an orderly arrangement of filaments and supporting matrix in the BM.

In the arcuate zone, the BM appears as a filamentous layer next to the feet of the pillar cells and a ground substance layer next to the scala tympani (Fig. 2F). However, in *Emilin2*$^{-/-}$ mice, the arcuate zone was dominated by filaments. The arcuate zone also includes the residual structure of the spiral vessel below the BM. This vessel is prominent in newborns but loses its role in blood flow in juvenile

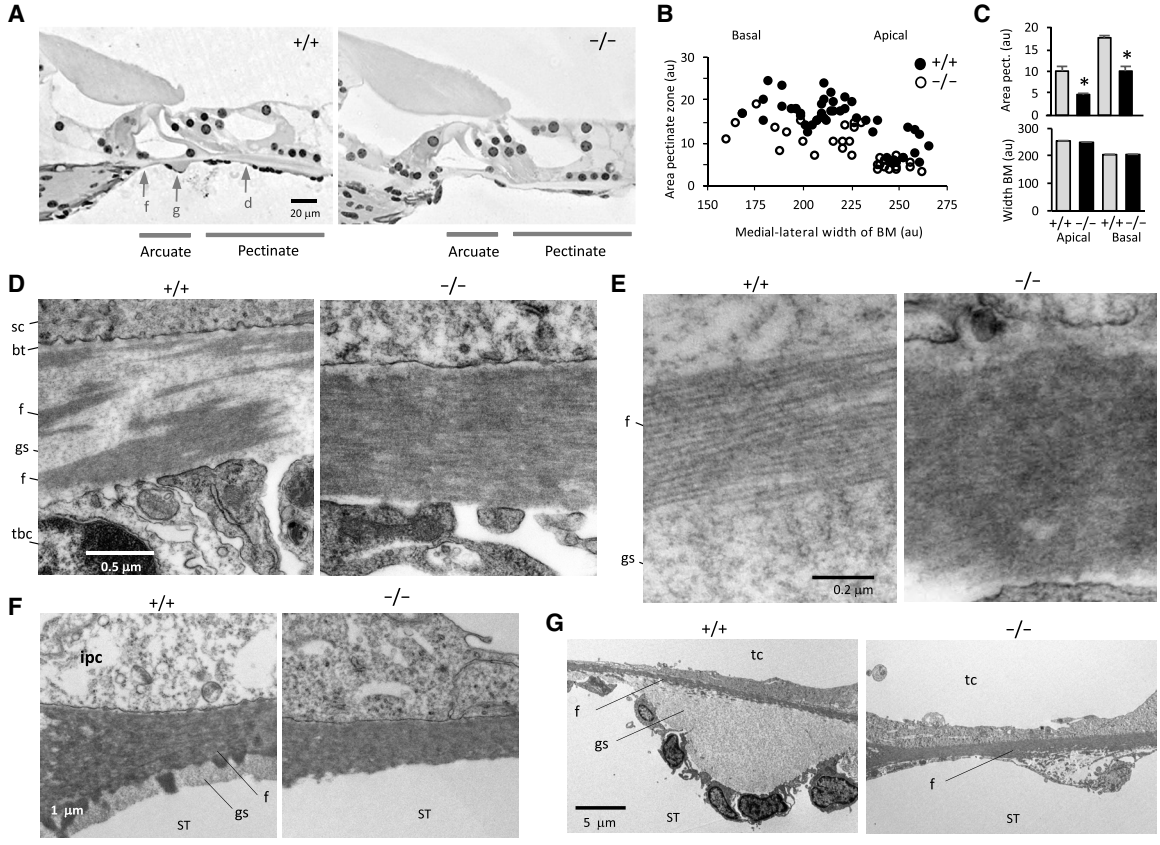

Fig. 2. Disarray of BM architecture in *Emilin2*$^{-/-}$ mice. (**A**) Intact organ of Corti in *Emilin2*$^{-/-}$ mice (6 months old; mid-turn histological sections). The spiral vessel structure is diminished. Arrows d, f, and g indicate views in (D), (F), and (G), respectively. (**B**) Compacted BM in *Emilin2*$^{-/-}$ mice [cross-sectional area of pectinate zone relative to width of arcuate-pectinate zone; $n = 6$ mice, 1 month old; 8 to 10 cochleae; views: +/+ basal 30, apical 14; *Emilin2*$^{-/-}$ basal 20, apical 17 (au, arbitrary units)]. (**C**) BM width and thickness [means ± SEM; asterisk (*), apical: $t = 5.227$, df = 29, $P = 0.00001348$; basal: $t = 6.351$, df = 50, $P = 0.000000062$, two-tailed t test; from data in (B)]. (**D** and **E**) Transmission electron micrographs [pectinate zone (mid-basal turn)]. Filaments (f) are normally interspersed in ground substance (gs). *Emilin2*$^{-/-}$ mice have denser filaments and less gs (3 months old). (**F**) Arcuate zone below inner pillar cell (ipc) shows loss of gs in *Emilin2*$^{-/-}$ mice. (**G**) The spiral vessel normally fills with gs, but gs is lacking in *Emilin2*$^{-/-}$ mice. bt, basement membrane; sc, support cell of sensory epithelium; ST, scala tympani.

mice (*17*). A residual structure is retained primarily in the middle and basal cochlea in older mice and becomes filled with ground substance (Fig. 2G), as has been described also for chinchilla (*10*). However, in *Emilin2*$^{-/-}$ mice, the residual structure was diminished and contained filamentous material rather than ground substance (fig. S2).

The overall integrity of the BM in *Emilin2*$^{-/-}$ mice was preserved on the basis of staining of extracellular matrix markers including emilin 1 (*12*), which displayed a similar pattern as emilin 2, and collagen IV, which localized to the basement membrane adjacent to the sensory epithelium (*18*) in both +/+ and *Emilin2*$^{-/-}$ mice.

To visualize the arrangement of the collagenous filaments in the BM, we used a form of polarized light microscopy that takes advantage of the anisotropy of the refractive index (birefringence) of structures. Thin optical sections of pieces of acutely isolated, unfixed BM were used to measure the orientation of the fibers as the slow optical axis of birefringence (*19*, *20*), which could be quantified according to a color wheel that shows a visual vectorial representation of orientations (Fig. 3A). The arbitrary orientation of BM pieces in each preparation resulted in color differences between preparations. However, within a given +/+ preparation, the fiber color was constant, indicating uniform alignment of fibers within the preparation, as shown for a mid-turn +/+ preparation in Fig. 3A. In contrast, in *Emilin2*$^{-/-}$ mice, this uniformity was disturbed, as indicated by the varied colors of fibers within a preparation. The histograms in Fig. 3B depict the wider range of orientations measured in *Emilin2*$^{-/-}$ than +/+ preparations in apical, middle, and basal turns of the cochlea. The wider distribution of fiber orientations in *Emilin2*$^{-/-}$ mice is indicated by the considerably greater SDs of the data.

The thickness and spacing of fibers and bundles of fibers also showed increases in *Emilin2*$^{-/-}$ compared to +/+ preparations, consistent with the disorder of these structures (Fig. 3, C to F). In apical regions, the optical imaging technique detected fibers but not bundles of fibers, consistent with the sparser presence of collagenous filaments in apical compared to mid-basal regions of the BM, as shown by electron microscopy (*4*, *5*).

Stacks of optical sections were used to reconstruct the filamentous array of the BM in longitudinal transverse views through the pectinate zone (Fig. 3G). In +/+ mice, the reconstruction showed vertically oriented fiber bundles. This pattern can occur if the radial bundles are arranged immediately above each other, similar to stringer supports inside an aircraft wing. In *Emilin2*$^{-/-}$ mice, the pattern appeared warped or braided with an offset arrangement of bundles, which was more apparent in thicker, mid-basal turns than in thinner

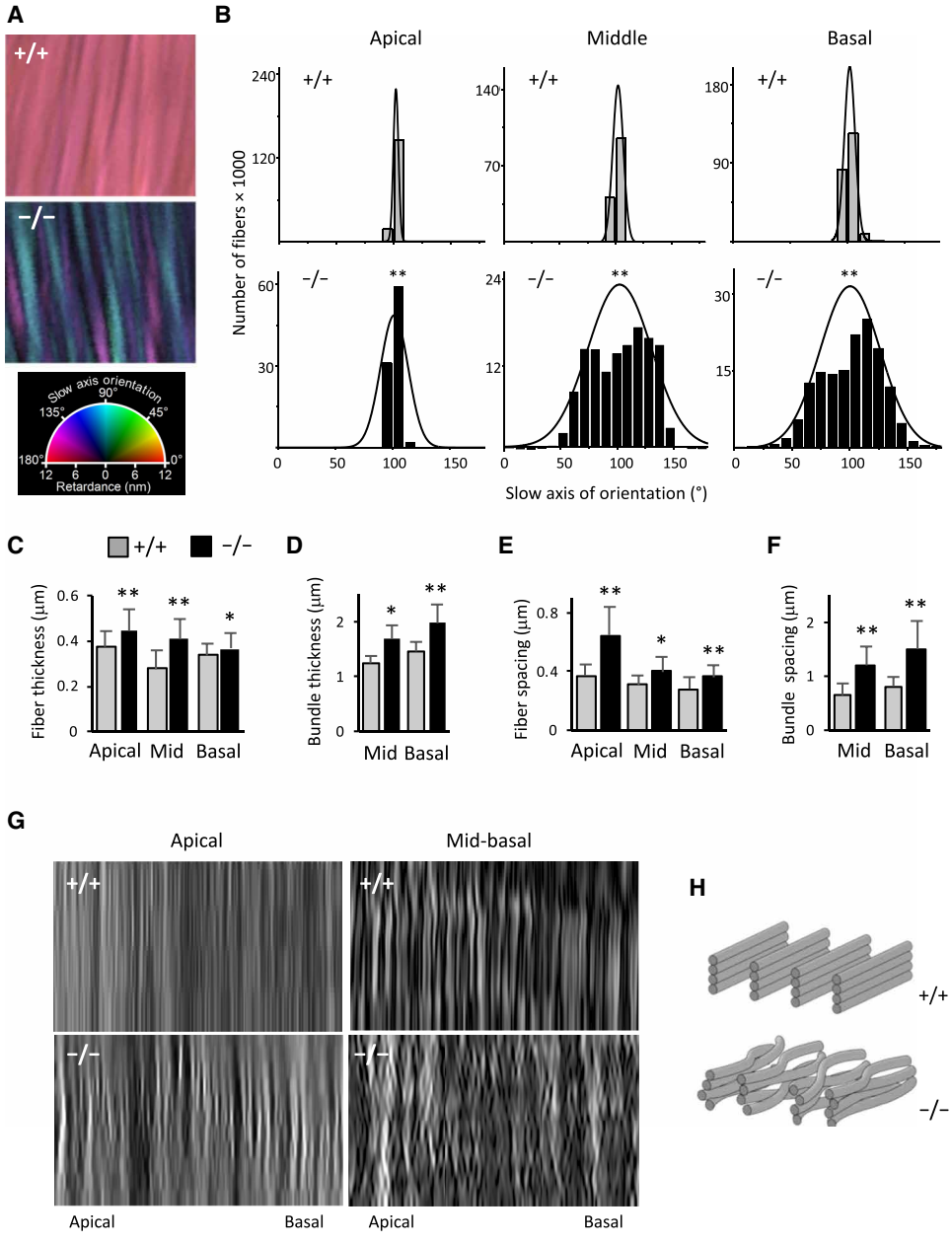

Fig. 3. Optical imaging of collagenous fibers in unfixed BM preparations. (**A**) LC-PolScope images of fibers and color wheel for quantification. Similar fiber colors for +/+ indicate uniform alignment; varied colors for *Emilin2*$^{-/-}$ indicate nonuniformity (10 μm by 10 μm views, mid-turn examples). (**B**) Range of relative fiber orientations in apical, middle, and basal turns. Fiber measurements were assigned to 10° bins (for fiber numbers, see Materials and Methods). Mean orientation in each preparation was normalized (to ~101°). Histograms were fitted with normal distribution curves. SD from the mean: apical, 2.2 (+/+) and 11.9 (−/−); middle, 4.7 (+/+) and 28.1 (−/−); and basal 4.7 (+/+) and 26.2 (−/−). Groups, three mice (six cochleae); differences in SD, $^{**}P < 0.0001$, *F* test statistics. (**C** to **F**) Fiber and fiber bundle thickness and spacing. Bundles were not observed in apical turns. Groups, three mice, means ± SD, $^{*}P < 0.001$ and $^{**}P < 0.0001$, two-tailed unpaired *t* test. (**G**) Filament array images reconstructed from stacks of pectinate zone optical sections (0.5 μm apart; 8 apical and 18 middle optical sections; total thicknesses are 4 and 9 μm, respectively). (**H**) Interpretative diagram showing an orderly array in +/+ mice and braided appearance in *Emilin2*$^{-/-}$ mice.

apical turns of the BM. The warped arrangement is depicted schematically in Fig. 3H.

BM frequency tuning in *Emilin2*$^{-/-}$ mice is multipeaked and shifted to lower frequencies

To investigate functional consequences of the disturbed BM architecture caused by absence of emilin 2, we analyzed frequency tuning using a self-mixing laser diode interferometer (*21*) to measure tone-evoked displacements of the BM for *Emilin2*$^{-/-}$ and +/+ littermates. Figure 4A shows a typical isoresponse, threshold displacement frequency tuning curve for a +/+ mouse measured at the 56-kHz characteristic frequency (CF) location on the BM. The curve is plotted as the threshold in decibel sound pressure level (dB SPL; 0 dB SPL = 20 μPa and 20 dB SPL = 200 μPa) required to achieve a 0.3-nm displacement

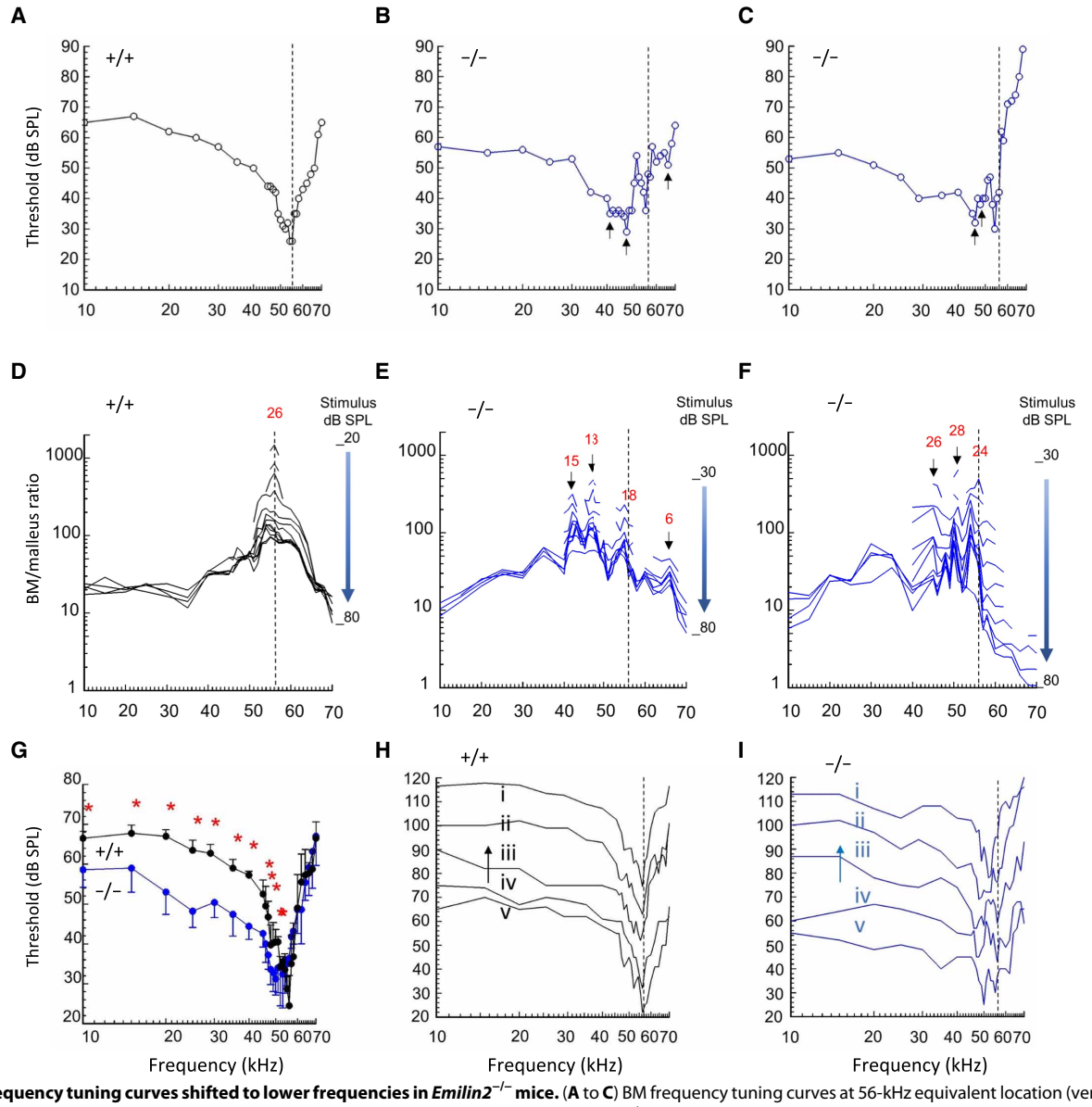

Fig. 4. BM frequency tuning curves shifted to lower frequencies in *Emilin2*$^{-/-}$ mice. (**A** to **C**) BM frequency tuning curves at 56-kHz equivalent location (vertical dashed line). BM threshold displacements (0.3-nm criterion) as functions of stimulus frequencies. *Emilin2*$^{-/-}$ mice are less sensitive to a 56-kHz tone and have broader, multipeaked responses (arrows). (**D** to **F**) BM/malleus displacement ratios [from data in (A) to (C)] as functions of stimulus level in 5-dB steps. Dashed lines, 56-kHz reference; arrows, additional peaks coincident with additional tuning curve minima for −/− mice. Red numbers, cochlear amplification (in dB) at peaks, calculated as the difference in BM/malleus displacement ratio for active (+/+, 20 dB SPL; −/−, 30 dB SPL) and passive (80 dB SPL) responses. (**G**) Mean tuning curves for five +/+ (black) and five −/− (blue) mice from three litters (mean and SD) showing more sensitive low-frequency tails for −/− mice (*$P < 0.05$, each point in range). At 56 kHz, +/+ mice were more sensitive ($t = 6.0867$, df = 8, $P = 0.0033$). (**H** and **I**) Irregular tuning curve shapes for five *Emilin2*$^{-/-}$ mice compared to five +/+ mice. Curves i, ii, iii, and iv are each incremented up (arrow) by 15 dB SPL from curve below.

of the BM, as a function of sound stimulus frequency. The curve has a well-defined, single minimum threshold peak in response to a 56-kHz tone with sharply rising thresholds for lower and higher frequencies and an insensitive, gradually sloping low-frequency tail. The curve resembles those that we have reported elsewhere (*22*). Curves of individual mice were plotted without data smoothing and showed small glitches in threshold, never exceeding 5-dB deviation from the mean, in the low- and high-frequency slopes of the curve. The curves, however, were consistent between mice, as reflected in the small SDs of +/+ group data (Fig. 4G, black curve) and similar peak shapes for different mice (Fig. 4H). The sensitivity, indicated by the threshold of the minimum tip of the mean curve, is 24.50 ± 3.75 dB SPL (means ± SD, $n = 10$). The sharpness of tuning of these curves, calculated by Q_{10dB} (equal to CF/10-dB bandwidth), is 11.3 ± 2.7 (means ± SD), on the basis of bandwidths measured 10 dB above the tip (means ± SD; 5.2 ± 1.3 kHz; range, 4 to 7 kHz).

The isoresponse frequency tuning curves for *Emilin2*$^{-/-}$ mice recorded at the 56-kHz equivalent location (*23*) displayed multiple minimal threshold peaks (typically two peaks) in contrast to the single peak in +/+ mice (Fig. 4, B and C). These minima mostly occurred

on the low-frequency slope of the curve, effectively sensitizing and shifting the responses. Most of the individual curves have a major peak 5 to 12 kHz below 56 kHz and a smaller peak within 1 to 2 kHz of the 56-kHz frequency. In those curves with only a single minimum, the peak centers in a region 5 to 11 kHz below the 56-kHz CF. The multipeak curves of *Emilin2*$^{-/-}$ mice (Fig. 4, B, C, and I) have a broader 10-dB mean bandwidth (means ± SD, 11.28 ± 3.73 kHz, n = 7) than the single peaks of +/+ mice (5.2 ± 1.3 kHz, n = 10; t = 4.8100, df = 15, P = 0.002, two-tailed unpaired t test). Responses in *Emilin2*$^{-/-}$ mice were notably inconsistent as indicated by the large SDs of the mean curve in Fig. 4G (blue curve, for the five mice represented in Fig. 4I), which has a minimum at 50 kHz with a tip threshold of 32.20 ± 4.00 dB SPL (means ± SD). The mean curve for another five *Emilin2*$^{-/-}$ mice [used to compare active and passive responses in Fig. 5 (B and D)] has minima at 48 kHz (threshold, 37.26 ± 6.65 dB SPL) and 56 kHz (threshold, 35.25 ± 4.11 dB SPL), again with large deviations. The results demonstrate that *Emilin2*$^{-/-}$ mice have an inconsistent relationship between a given BM location and its frequency response together with a downward frequency shift and loss of sensitivity (~10 dB SPL) at the 56-kHz equivalent place. However, the frequency tuning of the irregular peaks in the 47- to 56-kHz region is as sharply tuned as that of the 56-kHz peak of +/+ littermates with Q_{10dB} ranging from 9.4 to 18.7 (means ± SD, 12.5 ± 4.5) for the five individual curves in Fig. 4I. The results suggest that emilin 2 determines the precision and consistency of the BM frequency-place map.

Cochlear amplification extended to low frequencies in *Emilin2*$^{-/-}$ mice

It is widely accepted that the remarkable sensitivity of mammalian hearing depends on critically timed forces generated by outer hair cells that amplify vibrations of the BM in response to low-to-moderate SPLs close to threshold for frequencies around the CF [e.g., (*2*)]. For the frequency tuning curves in Fig. 4G, amplification of BM responses at the CF (56 kHz) is more effective for +/+ mice than *Emilin2*$^{-/-}$ mice [thresholds: 24.5 ± 5.2 dB SPL (+/+) and 35.3 ± 4.1 dB SPL (*Emilin2*$^{-/-}$); n = 5, t = 3.6469, df = 8, P = 0.0065]. However, for frequencies below the CF, e.g., on the low-frequency slope at 45 kHz, *Emilin2*$^{-/-}$ mice were significantly more sensitive (42.6 ± 3.4 dB SPL) than +/+ mice (52.5 ± 3.5 dB SPL; t = 4.5367, df = 8, P = 0.0019). Thus, in the absence of emilin 2, the BM may be more compliant than normal, and/or cochlear amplification may extend to lower frequencies at the 56-kHz equivalent location on the BM.

Passive stiffness (compliance) is a linear phenomenon and is independent of stimulus level, whereas cochlear amplification is an active, nonlinear process and is greatest for low-level stimulation. To investigate these two possibilities, we plotted the amplitude ratio (in dB SPL) between BM displacement in the cochlea (output) and malleus displacement in the middle ear (input). The ratio is independent of stimulus level if BM displacement is governed by compliance but is strongly dependent on stimulus level if governed by cochlear amplification. Ratio plots in Fig. 4 (D to F) show stimulus levels stepped (5-dB steps) from 20 to 80 dB SPL for a +/+ mouse (Fig. 4D) and from 30 to 80 dB SPL for two individual *Emilin2*$^{-/-}$ mice (Fig. 4, E and F). At low-level stimulation, BM displacements can be detected above the measurement noise floor (~0.04 nm) only over a limited frequency range centered on the sensitive peaks of the BM frequency tuning curve (Fig. 4, A to C), which results in the incomplete or broken curves for low SPL measurements (Fig. 4, D to F).

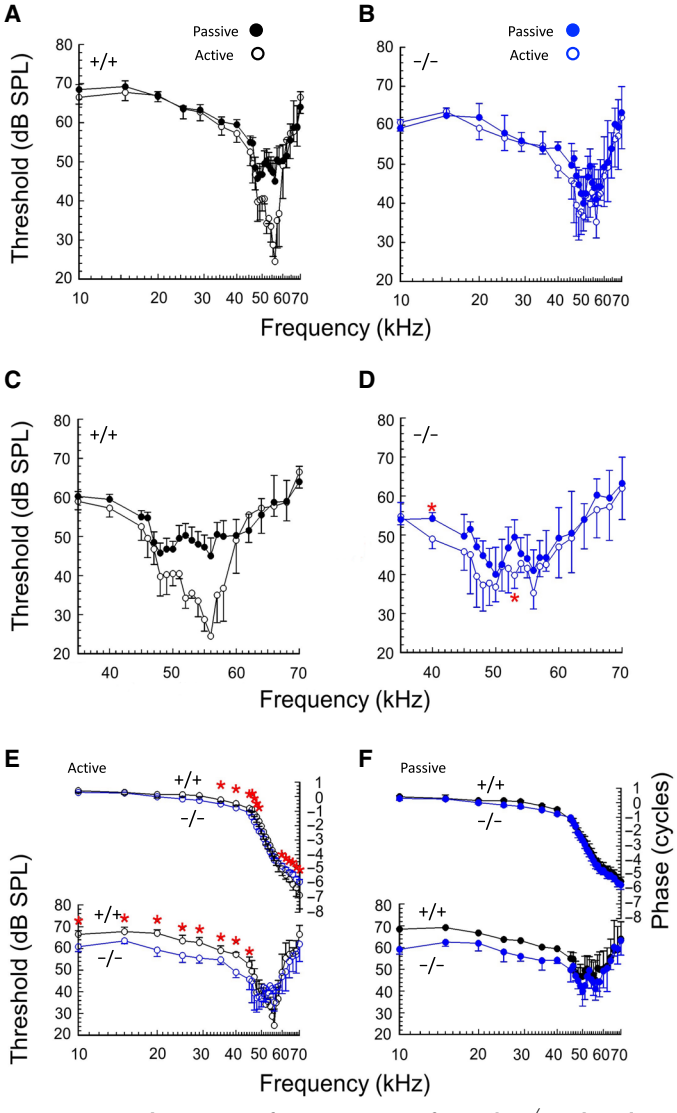

Fig. 5. Active and passive BM frequency tuning for *Emilin2*$^{-/-}$ and +/+ littermates. (**A** and **B**) Mean displacement thresholds for active (open symbols) and passive (postmortem; solid symbols) responses (n = 5, two different litters from groups in Fig. 4). Mean and SD; BM threshold displacement (0.3-nm criterion) at 56-kHz equivalent place. The 56-kHz peak is lost postmortem in +/+ mice; irregular peaks persist in *Emilin2*$^{-/-}$ mice. (**C** and **D**) Expanded 35- to 70-kHz region from (A and B). For +/+, pre- and postmortem responses differed over 45 to 58 kHz (P < 0.001, each point). For *Emilin2*$^{-/-}$, peaks remained at 56 and ~50 kHz; large variations between mice yielded significant differences (*) in mean curves only at 40 kHz (t = 4.0468, df = 8, P = 0.0038) and 53 kHz (t = 3.9450, df = 8, P = 0.0042). (**E** and **F**) BM displacement thresholds (y axis, left) and phase (y axis, right; 50–dB SPL stimulus) as functions of stimulus frequency. Low-frequency responses (10 to 45 kHz) were significantly less sensitive for +/+ than *Emilin2*$^{-/-}$ mice. Displacement phase for *Emilin2*$^{-/-}$ mice significantly lagged +/+ mice at <47 kHz and led at >58 kHz, indicating reduced BM stiffness in *Emilin2*$^{-/-}$ mice. *$P \leq 0.005$, two-tailed unpaired t test.

For higher stimulus levels (>60 dB SPL), amplification disappears and the BM/malleus ratio is insensitive to changes in stimulus level up to the maximum used (80 dB SPL). Compared to +/+ mice, the ratio in *Emilin2*$^{-/-}$ mice is very irregular for frequencies above ~40 kHz, indicating irregularities in BM mechanical properties.

In +/+ mice, the greatest change in ratio occurs at the CF, indicated by the dashed line at 56 kHz in Fig. 4D. For this +/+ mouse, the ratio or amplification is 26 dB (red number above 56-kHz line) and the mean amplification ± SD for six +/+ preparations is 27.2 ± 5.7 dB. However, in *Emilin2*$^{-/-}$ mice, changes in ratio were also evident at the additional sensitivity peaks of the BM frequency tuning curves (arrows; Fig. 4, B, C, E, and F). The ratio or amplification is noted (red numbers, dB) above the arrows and the 56-kHz line. The mean amplification ± SD for 15 peaks (between 42 and 56 kHz) in five *Emilin2*$^{-/-}$ preparations is 17.4 ± 7.5 dB. Thus, the low-frequency boundary for cochlear amplification for *Emilin2*$^{-/-}$ mice extends to frequencies below normal at the 56-kHz equivalent place (Fig. 4D). Overall, the tuning curve peaks of *Emilin2*$^{-/-}$ mice are significantly less sensitive than those of +/+ mice ($t = 17.8692$, df = 19, $P = 0.0098$), but the ratio of amplification of the additional, irregular peaks in *Emilin2*$^{-/-}$ mice can approach that of +/+ mice.

Cochlear amplification disappears postmortem such that comparison of pre- (active) and postmortem (passive) BM responses indicates the frequency range of amplification and its contribution to the shape of the BM frequency tuning curves. For +/+ mice (Fig. 5A and expansion in Fig. 5C), the minimal threshold peak at 56 kHz was lost postmortem [means ± SD, 24.5 ± 3.7 dB SPL (active) and 49.6 ± 4.2 dB SPL (passive); $P < 0.0001$, df = 8, t = 10.0272]. The amplification range spanned between 45 and 58 kHz. In contrast, for *Emilin2*$^{-/-}$ mice, the two minima at 56 kHz and in the 47- to 50-kHz region (Fig. 5, B and D) remained postmortem, suggesting irregularities in the passive mechanical properties of the BM. For *Emilin2*$^{-/-}$ mice, thresholds at both frequency regions did increase somewhat postmortem, but because of large deviations, differences did not consistently reach significance compared to the marked change in +/+ mice. Differences were significant in the low-frequency range at 40 kHz for *Emilin2*$^{-/-}$ mice [Fig. 5D; means ± SD, 49.00 ± 2.48 dB SPL (active) and 54.25 ± 1.50 dB SPL (passive); $t = 4.0504$, df = 8, $P = 0.0037$]. Both active and passive thresholds at 40 kHz were lower for *Emilin2*$^{-/-}$ mice than +/+ mice (both thresholds for +/+ were close to 60 dB SPL; Fig. 5C).

Together, these results indicate that in *Emilin2*$^{-/-}$ mice, BM stiffness is irregular but, overall, the BM is more compliant and that amplification extends to lower frequencies with additional tuning peaks involving active amplification.

Enhanced sensitivity of low-frequency tuning in *Emilin2*$^{-/-}$ mice

Thresholds of the low-frequency tail of the BM tuning curves in the 10- to 40-kHz region were, on average, 6.38 ± 1.51 dB lower for *Emilin2*$^{-/-}$ mice than +/+ mice (Fig. 5E). This unusual sensitivity of the low-frequency tail suggested decreased stiffness of the BM for *Emilin2*$^{-/-}$ mice, which was corroborated by analysis of BM phase. The phase of BM displacements measured 15 dB above displacement threshold indicated that the phase for *Emilin2*$^{-/-}$ mice significantly lagged that for +/+ mice at frequencies below 47 kHz but led for frequencies above 57 kHz (Fig. 5E; upper phase cycle curves). The phase lag for frequencies <45 kHz, a range in which BM responses are dominated by stiffness, remained postmortem (Fig. 5F), providing additional evidence that passive BM stiffness is less for *Emilin2*$^{-/-}$ mice than +/+ mice. Together, the results indicate that emilin 2 is required for the smooth mechanical function and stiffness of the BM that mediate effective amplification of responses at a defined frequency place on the BM.

According to Müller *et al.* (*23*), the distance of the characteristic place from the base of the cochlea (as percent of total length of the BM) as a function of CF on a logarithmic scale shows a linear decrease of distance *d*, with frequency *f*, given by $d = 156.5$ to $82.5 \log f$. Thus, the shift of a dominant peak in *Emilin2*$^{-/-}$ mice to ~47 kHz at the 56-kHz equivalent place suggests a basal-ward shift of the 47-kHz place from 18.55 to 12.27% of the length of the BM (from cochlear base). Given a total length of the mouse BM of ~5.13 mm along the row of inner hair cells, the calculation suggests that the characteristic place for ~47 kHz has shifted or spread ~0.32 mm basal-ward in *Emilin2*$^{-/-}$ mice.

Alteration of neural masking tuning curves of *Emilin2*$^{-/-}$ mice

The neural consequences of the altered mechanical function of the BM in *Emilin2*$^{-/-}$ mice were investigated at the level of the auditory nerve by analysis of neural masking tuning curves. We measured the threshold of masker tones required to suppress compound action potential (CAP) responses to specific probe tones at 12 and 20 kHz. Higher frequencies were not used because suppression tuning curves in the 50- to 60-kHz region could be subjected to fatigue of the neural responses. Simultaneous neural CAP masking tuning curves recorded from the cochlear round window closely resemble neural tuning curves recorded from single auditory nerve fibers [e.g., (*24*)]. Compared to the neural masking CAP tuning curves recorded from +/+ mice (Fig. 6A), the curves for *Emilin2*$^{-/-}$ mice displayed elevated, less sensitive masker thresholds at the probe frequency and broadened responses at other frequencies (Fig. 6B). The broadened responses resembled those of the mechanical BM tuning curves of *Emilin2*$^{-/-}$ mice (see Fig. 5) but were less erratic, consistent with the operation of additional, natural filtering mechanisms that modify neural responses. Additional peaks were evident in the neural masking tuning curves in *Emilin2*$^{-/-}$ mice, most clearly at ~12 kHz for the 20-kHz probe tone (Fig. 6B). Averaged data for mice with similar (±3 dB SPL) probe tone levels showed that compared to +/+ mice, the simultaneous neural masking tuning curves for *Emilin2*$^{-/-}$ mice were less sensitive at the probe tone and more broadly tuned with high- and low-frequency skirts in the curves (Fig. 6, C and D).

Elevation of distortion product otoacoustic emission and auditory-evoked brainstem response thresholds in *Emilin2*$^{-/-}$ mice

Distortion product otoacoustic emissions (DPOAEs) recorded in the ear canal are acoustic, nonlinear cochlear responses to simultaneous stimulation with two pure tones, f1 and f2. Cubic distortion (2f1 – f2) is usually the dominant DPOAE and is a consequence of the nonlinear properties of mechanosensory transduction mechanisms (*25*) and cochlear amplification (*26*). Therefore, DPOAE threshold as a function of f2 stimulus frequency indicates the sensitivity and frequency range of cochlear responses at the level of the outer hair cells, which also depends on the mechanical properties of other cellular and membranous structures of the cochlear partition. The aberrant BM function in *Emilin2*$^{-/-}$ mice might accordingly be associated with changes in DPOAEs. For frequencies between 15 and 60 kHz, DPOAE thresholds for *Emilin2*$^{-/-}$ mice were 10 to 25 dB SPL higher than those of +/+ mice (fig. S3), which might result from the reduced cochlear amplification and not to any significant influence of the mutation on the ascending auditory pathway in *Emilin2*$^{-/-}$ mice.

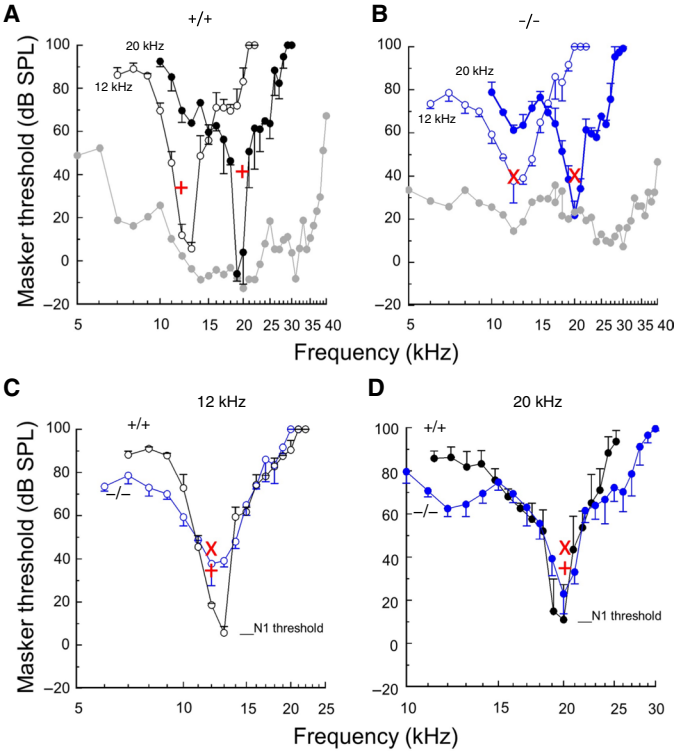

Fig. 6. Simultaneous masking neural frequency tuning curves. (**A** and **B**) Masker tone thresholds required to suppress CAP threshold response to probe tones as functions of masker tone frequency: +/+ [(A), black] and *Emilin2*$^{-/-}$ [(B), blue] for 12 kHz (open symbols) and 20 kHz (solid symbols) probe tones. Each point: means ± SD of 10 measurements. Gray symbols, CAP threshold audiograms. (**C** and **D**) Mean curves (±SD) for five mice. Dashed horizontal line, CAP threshold at probe tone frequency for +/+ (N1 threshold). Responses are significantly less sensitive for *Emilin2*$^{-/-}$ than +/+ mice. Minima for 12-kHz probe tone (C): +/+, 5.7 ± 4.2 dB SPL and –/–, 37.7 ± 14.4 dB SPL ($t = 4.7703$, df = 8, $P = 0.0014$). Minima for 20-kHz probe tone (D): +/+, −4.8 ± 6.3 dB SPL and –/–, 22.9 ± 9.2 dB SPL ($t = 5.5549$, df = 8, $P = 0.0005$). *Emilin2*$^{-/-}$ 20-kHz curves are broader with minima on high- and low-frequency slopes. Q_{10dB} (probe tone frequency/bandwidth of 10 dB from tip) for 12-kHz probe tone: +/+, 5.4 and –/–, 2.4; for 20-kHz probe tone: +/+, 14.3 and –/–, 11.1. Red "+" (+/+) and "x" (–/–) symbols are probe tone frequency and SPL, respectively.

It may be anticipated that any mechanical discontinuity in the BM of *Emilin2*$^{-/-}$ mice could generate spontaneous otoacoustic emissions (SOAEs) since deformity of the tectorial membrane, the other major extracellular membranous structure of the organ of Corti, produces SOAEs (*27*). However, SOAEs were not detected in *Emilin2*$^{-/-}$ mice, suggesting that changes in the properties of the tectorial membrane rather than the BM cause the most disruption to energy exchange between the outer hair cells and other structures of the cochlear partition. The observation also implies that the BM is more closely associated with energy input to the cochlear partition, whereas the tectorial membrane is more closely associated with directed energy output.

Measurement of the auditory-evoked brainstem response, an indicator of overall auditory function, showed moderately elevated thresholds in *Emilin2*$^{-/-}$ mice compared to +/+ mice for a click stimulus and a range of specific frequencies (8, 16, and 32 kHz; fig. S3, B and C). The results may be consistent with the elevated thresholds for the DPOAE and suggest the absence of additional, major defects in the auditory pathway.

DISCUSSION

We report a key role for emilin 2 in promoting the mechanical properties of the BM and the ability to distinguish frequencies in sound. *Emilin2*$^{-/-}$ mice display broadened mechanical frequency tuning and neural tuning with irregular peaks shifted to frequencies below normal at a given location on the BM. Our findings suggest that emilin 2 organizes the collagenous filament array in the BM to promote a stiffness gradient that is critical for an accurate frequency-place map. Less stiffness may make basal regions functionally more like middle-apical regions of the BM in allowing responses to lower frequencies. However, the irregularity of the additional peaks indicates that emilin 2 is also required to confer consistency and precision on the response.

Consistency of mechanical tuning and stiffness of the BM

The changes in BM mechanical responses in *Emilin2*$^{-/-}$ mice that indicate reduced BM stiffness [e.g., (*28*, *29*)] include a downward frequency shift of the major response peak and increased sensitivity and phase lag in the low-frequency tails of the BM tuning curves. A notable finding is that the BM tuning curves are not only shifted to lower frequencies but also differ between individual *Emilin2*$^{-/-}$ mice with respect to the location and shape of peaks. This inconsistency of response is in marked contrast to the consistency of the major, single response peak observed in normal curves in control mice. Accuracy in the frequency-to-place map is essential for meaningful perception of sounds and for communication between individuals, which require that the BM reliably mediates stereotyped responses for a given frequency. Our findings indicate that emilin 2 is critical for the consistency of this response.

Our results show that emilin 2 promotes the arrangement of the radial collagenous filaments in the ground substance of the BM, suggesting that evenly aligned and spaced filaments are necessary for the finely calibrated elasticity of the BM. Emilin 2 has several protein-binding domains such as a C1q globular domain (*12*), suggesting that it interacts with other proteins to promote the specialized architecture and stiffness of the BM. Emilin 2 in the ground substance (*12*) may serve to space and prevent warping of the collagenous filaments. However, elucidation of the emilin 2–mediated protein interactions in the matrix awaits better knowledge of other components of the BM and how these are assembled. Emilin 2 has been reported to associate with extracellular matrices in skin (*13*) and to influence extracellular signaling during blood clotting (*16*) and tumor angiogenesis (*15*). The interactions of emilin 2 in the BM may be unique given the exquisite mechanical sensitivity of this specialized structure that underlies auditory frequency resolution.

An orderly filamentous configuration in the ground substance matrix may allow the smooth progression of the traveling wave along the BM that leads to frequency-specific excitation (*30*). We speculate that emilin 2 constrains the spread of mechanical excitation to demarcate a place of maximal response on the BM as required for high-resolution frequency tuning. The precision of these frequency responses presumably reflects the influence of the filamentous array on the overall stiffness of the BM in both radial and longitudinal orientations.

A possible limitation of the study is that for reasons of accessibility, the mechanical measurements of BM frequency tuning were confined

to basal (high frequency) regions of the cochlea. However, emilin 2 protein is present along the full length of the BM, suggestive of a similar role over the entire cochlear frequency map. In support of this proposal, *Emilin2*$^{-/-}$ mice displayed similar subtle thinning of the BM and compaction of the spiral vessel in all turns of the cochlea, while optical imaging indicated the presence of disordered collagen fibers in all turns. Functionally, the DPOAE audiogram (fig. S3A) revealed reduced sensitivity over a wide range of frequencies, as would be expected for a general loss of frequency resolution with moderately elevated thresholds along the cochlear length. Similarly, auditory-evoked brainstem responses were moderately elevated in *Emilin2*$^{-/-}$ mice (fig. S3, B and C).

Emilin 2 and the smooth mechanical gradient of the BM

It may be assumed that a smooth gradient of BM mechanical responses is required for fine resolution of frequencies. In *Emilin2*$^{-/-}$ mice, the multipeaked rippling near the CF place on the BM tuning curves suggests a disrupted mechanical gradient [e.g., (*9*, *31*)], and the shallow phase slopes suggest abnormal spread of excitation along the BM (*29*).

In a hypothetical mechanically ordered cochlea, the traveling wave energy is dissipated on its way to the CF place. The cochlea, however, is not a perfectly smooth transmission line, and traveling wave energy may be partially backscattered because of random mechanical irregularities along the cochlear partition (*32*). Wave reflection and interference may contribute to the generation of DPOAEs [e.g., (*33*, *34*)] and to transient evoked otoacoustic emissions [e.g., (*35*)]. To date, an anatomical or molecular basis for mechanical irregularities in cochlear function is unknown. However, the cochlea is a biological organ rather than a perfect mechanical structure. Natural variations in the precise cellular array of the organ of Corti or in the ultrastructure of the BM along the length of the cochlea might produce slight functional variations that contribute to rippling and limits on frequency resolution. It is possible that small perturbations in normal hearing thresholds (*31*) are phenomenologically similar to the exaggerated ripples in the BM tuning curves of *Emilin2*$^{-/-}$ mice. Potentially, the disorganized BM in *Emilin2*$^{-/-}$mice exacerbates these irregularities to produce wave reflections and interference that exaggerate the ripples in cochlear responses (*31*). Thus, abnormalities in *Emilin2*$^{-/-}$ mice may effectively broaden cochlear frequency tuning and compromise frequency resolution by the hearing periphery. A smooth BM gradient would not only provide efficient mechanical energy transmission within the cochlea but also discrete resolution of cochlear frequency tuning.

Emilin2 and neural masking tuning curves

Our findings indicate that emilin 2–dependent functions of the BM are critical for accurate neural transmission of frequency information. Precision in cochlear frequency resolution is a prerequisite for the peripheral coding of auditory frequency information. *Emilin2*$^{-/-}$ mice display broadening of neural masking frequency tuning curves and insensitivity at the probe tone, implying that *Emilin2*$^{-/-}$ mice are less able to discriminate between frequencies.

Neural responses measured at the level of the auditory nerve reflect the activities of the inner hair cells and their afferent innervation, which are filtered dynamically by cellular (e.g., outer hair cell) and noncellular structures of the cochlear partition. In *Emilin2*$^{-/-}$ mice, a secondary peak of the neural masking tuning curves for the 20-kHz probe tone appears at ~12 kHz, close to the frequency of the tectorial membrane resonance [e.g., (*36*, *37*)], and indicates filtering by the tectorial membrane (*38*). The insensitivity at the probe tone frequency and abnormal sensitivity of the low-frequency shoulder for both 12- and 20-kHz probes and, in addition, of the high-frequency shoulder for the 20-kHz probe (Fig. 6) may indicate that inner hair cell responses have a more extensive inhibitory field of mutual suppression (*39*) than normal.

Vibrations at a given frequency place on the BM result in transverse shear between the tectorial membrane and reticular lamina to contribute to the excitation of inner hair cells at this place (*40*, *41*). However, the ability of the cochlear partition to filter out or amplify mechanical responses does not mean that strong, secondary frequency peaks in BM mechanical responses at a given location excite inner hair cells at this location. Other frequency components in the traveling wave may produce different modes of vibration of the organ of Corti to modify the excitation of inner hair cells at adjacent places [e.g., (*42*)]. A natural example of multiple frequency peaks arising at a single BM location occurs in the greater mustached bat. A specialized zone on the basal side of the place of the 61-kHz second harmonic component of the echolocation signal (*42*) produces tuned responses at 62 to 67 kHz and also a strong standing wave that excites inner hair cells at the adjacent 61-kHz frequency place.

An implication of our findings is suggested by reports that among mammalian species examined, humans have the most precise cochlear tuning and perceptual frequency discrimination (*3*) [apart from constant frequency bats (*43*)]. It would therefore be of interest to find if there are special molecular features of the human BM, possibly involving emilin 2, that account for this enhanced frequency tuning. Any deterioration of frequency tuning at the level of the BM, such as that mediated by emilin 2, may contribute to tone deafness or difficulties in perception of speech or sound in noisy environments. Defective cochlear frequency tuning might also contribute to the impaired auditory and language processing that can occur in developmental thyroid disorders (*44*) since *Emilin2* expression is impaired in thyroid hormone receptor-deficient mice (*12*).

MATERIALS AND METHODS

Mutagenesis and mouse strains

To generate an *Emilin2* null allele, *lacZ* was fused in-frame at the ATG start codon of the gene by homologous recombination in embryonic stem (ES) cells derived from C57BL/6J mice (Ozgene Pty Ltd., Western Australia). The *lacZ* cassette replaced the first two coding exons of the gene (*12*). Chimeric founders derived from recombinant ES cells were crossed to *Rosa26*^{Cre} mice to remove the loxP-flanked *Neo* selection gene. The *Rosa26*^{Cre} allele was removed by backcrossing with C57BL/6J mice (JAX, no. 000664). *Emilin2*$^{+/-}$ parents were intercrossed to generate +/+, +/−, and −/− mice for analysis. Genotypes were determined by polymerase chain reaction using three primers (Em2 forward, 5′-CCG AGC CCG CTG CCG; Em2 reverse, 5′-GGC AGA TCC CGT AGT TCT GCC G; and Bgal reverse, 5′-CCG CTT CTG GTG CCG GAA ACC), giving a wild-type band of 439 base pairs (bp) and a mutant band of 261 bp. For physiological measurements, mice were backcrossed for at least seven generations onto a CBA/CaCrl background (Charles River Laboratories, UK, no. 609) to minimize high-frequency hearing loss (*45*) at the University of Brighton. Mice were housed under standard conditions with 12-hour light/12-hour dark cycles with food and water ad libitum. Studies were performed in accordance with approved protocols at National

Institute of Diabetes and Digestive and Kidney Diseases (NIDDK) at the National Institutes of Health and with U.K. Home Office regulations with approval from the University of Brighton Animal Welfare and Ethical Review Body.

Immunostaining and histochemistry

Cochleae were dissected and fixed in 4% paraformaldehyde (PFA) for 1 hour for β-galactosidase assays or 3 hours for immunostaining. Cochleae (P8 and older) were decalcified in 100 mM EDTA (3 to 7 days at 4°C with change of buffer every 2 to 3 days), cryoprotected in 30% sucrose in phosphate-buffered saline (PBS), and then embedded in optimal cutting temperature material. For immunostaining, 12-μm cryosections were incubated in 1.5% goat serum, 0.1% bovine serum albumin (BSA), and 0.4% Triton X-100 in PBS and then incubated with first antibody in the same solution for 3 hours overnight (~15 hours) at room temperature. Antibodies (source; dilution) were as follows: emilin 2 and emilin 1 [(*12*); 1:2000], collagen IV (Abcam, ab6586; 1:1000) (RRID: AB_305584). Sections were incubated with secondary antibodies Alexa Fluor 448–conjugated goat anti-chicken (RRID: AB_142924) and/or Alexa Fluor 568–conjugated goat anti-rabbit (RRID: AB_143157). For whole-mount pieces of cochlea, after decalcification, the bony capsule, lateral wall, and modiolus were removed. The organ of Corti was incubated with anti–emilin 2 antibody overnight and then with Alexa Fluor 568–conjugated goat anti-rabbit antibody for detection. Images were captured on a Leica DMI4000 B-SC laser confocal microscope. Images were processed using Photoshop or ImageJ (see the "Software/code" section below). For β-galactosidase histochemistry, whole-mount cochleae (P8) were immersed for 2 hours in substrate solution containing 5-bromo-4-chloro-3-indolyl-β-D-galactopyranoside (1 mg/ml; X-gal; β-Galactosidase Reporter Gene Staining Kit, Sigma-Aldrich). Cochleae were postfixed in 4% PFA and decalcified, and the bony capsule was removed. Cochlear cryosections were incubated in the same X-gal substrate solution for 3 to 18 hours to detect signals.

Western blot analysis, protein expression, and cell transfection

Whole-cell protein lysates were made from pooled cochleae from 6 to 8 pups at P8. Cochleae were frozen at −80°C before pools were homogenized in radioimmunoprecipitation assay (RIPA) buffer [10 mM tris-HCl (pH 8.0), 140 mM NaCl, 0.5% Triton X-100, 1% sodium deoxycholate, and 0.1% SDS] and protease inhibitor cocktail (no. 11836145001, Sigma-Aldrich, USA) using a motor probe (Kimble Chase, 749540-0000). Experiments were performed on two independent pools. A control full-length emilin 2 cDNA was expressed in transfected human embryonic kidney (HEK) 293T cells. The cDNA was cloned from mouse brain mRNA using Phusion polymerase (New England Biolabs) and primers as follows: Em2-FlagF, 5′-ATG GAC TAC AAG GAC GAC GAT GAC AAG ATG TGT CAG GAG ACC CCG CCC-3′ and Em2–Mlu I–R, 5′-GAT CCT CGA GAC GCG TCT AGA GGT GAG AAA GGA AAG GG-3′. A second set of primers was used to introduce Mfe I and Mlu I enzyme sites for cloning into pCIG2-C1 expression vector: Flag–Mfe I–F, GAT CAC AAT TGT GGC CAC CAT GGA CTA CAA GGA CGA CGA TGA CAA G-3′ and Em2–Mlu I–R, as above. The cDNA was verified by sequencing. HEK 293T cells were cultured in Dulbecco's modified Eagle's medium containing 10% fetal bovine serum at 37°C and in 5% CO_2. Cells were transfected with plasmids using GenJet Plus In Vitro DNA Transfection Reagent (SignaGen Laboratories, USA). Two days after transfection, cells were lysed in RIPA buffer and protease inhibitor cocktail as for cochlear samples.

Proteins (20 μg from cochleae and 5 μg from transfected cells) were resolved by SDS–polyacrylamide gel electrophoresis and transferred to polyvinylidene difluoride membranes (Bio-Rad, USA). Membranes were incubated with primary antibodies [1:1000 anti–emilin 2 rabbit polyclonal (*12*) or anti–α-actin (monoclonal MAB1501, Millipore, USA; RRID: AB_2223041)] in 4% BSA in PBS containing 0.1% Tween 20 overnight at 4°C. Membranes were washed five times in 1× PBS containing 0.2% Tween 20 (PBST) and then incubated with a 1:10,000 dilution of horseradish peroxidase–linked anti-rabbit (G-21234, RRID: AB_2536530) or anti-mouse secondary (62-6520, RRID: AB_2533947) antibodies (Thermo Fisher Scientific, USA) for 1 hour at room temperature. After washing in PBST, detection was performed using enhanced chemiluminescence reagents. The membrane was reprobed for actin after stripping with Western Blot Stripping Buffer (46430, Thermo Fisher Scientific, USA).

Histology and transmission electron microscopy

For histology, cochleae were fixed in 2% PFA/3% glutaraldehyde, decalcified, dehydrated in a series of graded ethanols (30 to 100%), embedded in glycol methacrylate plastic, sectioned on a microtome at 4-μm thickness in the mid-modiolar plane, and then stained with hematoxylin, as described (*46*). Images were captured using a Nikon 80i microscope. Hair cells were counted, and thickness and area of the BM were measured on sections made from 8 to 10 cochlea (from six mice) using ImageJ (see the "Software/code" section below). Measurements were made on groups at ~1 month and at 3 months (not shown) of age. For transmission electron microscopy, after decalcification, the bony capsule was removed; then, pieces of cochlea were postfixed in 1% osmium tetroxide in PBS and embedded in Spurr's plastic resin. Pieces from middle or mid-basal cochlear regions were analyzed from groups of five mice at 2 to 3 months of age. Sections were analyzed on a Carl Zeiss transmission electron microscope (Jan Endlich, JFE Enterprise, University of Maryland, College Park, USA).

Birefringence imaging

Birefringence imaging allows observations in thin optical sections of acutely isolated, unfixed BM, thus avoiding artefacts associated with fixation. The technique uses anisotropy of the refractive index that, in birefringent materials, depends on the polarization of light and direction of its propagation. Temporal bones were isolated from mice (~P30) at NIDDK and shipped overnight to the Marine Biological Laboratory (MBL; Woods Hole, MA). Samples were shipped in ice-cold Leibovitz's medium (L-15 Medium; Thermo Fisher Scientific, catalog number 21083) and arrived at MBL within ~18 hours of harvesting. No difference was observed whether control samples were shipped from NIDDK or were isolated at MBL, suggesting that shipment of material did not change outcomes. At MBL, cochleae were isolated and the BM was dissected in ice-cold Leibovitz's medium. Samples of apical, middle, and basal turns of the cochlea were separated. Each section was examined in a drop of bath solution under a coverslip using a Nikon microscope with an oil immersion 60×/0.9 numerical aperture objective lens and equipped with a QImaging Retiga 2000R camera. LC-PolScope and Polychromatic PolScope were used to measure magnitude (retardance) and orientation (slow optical axis) of BM birefringence. Fiber orientations were determined using a color wheel. Images were analyzed using OpenPolScope and

other software (see the "Software/code" section below). Samples were imaged without knowledge of genotypes, which were confirmed later. Numbers of fiber orientations are measured in optical sections (0.5 μm apart; in Fig. 3B): apical, 163,805 (+/+) and 164,805 (−/−; in 8 optical sections); middle, 137,443 (+/+) and 134,658 (−/−; in 20 optical sections); and basal, 145,339 (+/+) and 151,419 (−/−; in 20 optical sections). Measured angles were assigned to 18 bins, each representing 10° of orientation. To compare preparations with varied absolute orientations, the mean orientation of each preparation was normalized (to ~101°) by shifting orientation lines (without altering distribution patterns). Differences between genotypes were most evident in mid/basal turns as the BM is thicker in this region and more amenable to LC-PolScope analysis, which has a lower limit of 0.5 μm. To test whether the orientation of fibers was significantly different between genotypes, we used the SD to calculate the coefficient of variance and then performed an *F* test using Origin software to test whether data samples came from populations with equal variances. Corresponding *P* values were determined from *F* test values using Origin. The thickness of fibers and fiber bundles was measured on images obtained from Photoshop (Adobe) and then analyzed using Origin software. The number of fibers or bundles was measured [in Fig. 3 (C to F); fiber thickness: apical, 135 (+/+) and 130 (−/−); middle, 151 (+/+) and 99 (−/−); and basal, 150 (+/+) and 147 (−/−); fiber bundle thickness: middle, 136 (+/+) and 125 (−/−) and basal, 75 (+/+) and 72 (−/−); fiber spacing: apical, 94 (+/+) and 91 (−/−); middle, 151 (+/+) and 101 (−/−); and basal, 150 (+/+) and 151 (−/−); fiber bundle spacing: middle, 151 (+/+) and 126 (−/−) and basal, 109 (+/+) and 90 (−/−); groups, three mice (six cochleae)].

Physiological recordings

Mice at 3 to 5 weeks of age were anesthetized with ketamine [0.12 mg/g body weight intraperitoneally (i.p.)] and xylazine (0.01 mg/g body weight, i.p.) for nonsurgical procedures or with urethane (ethyl carbamate; 2 mg/g body weight, i.p.) for surgical procedures at the University of Brighton. Mice were tracheotomized, and their core temperature was maintained at 38°C. To measure BM displacements, cochlear microphonics (CM), and CAPs, a caudal opening was made in the ventrolateral aspect of the right bulla to reveal the round window. CM and CAP were measured from the round window membrane using glass pipettes pulled from 1-mm-diameter borosilicate tubing on a Sutter P-2000 micropipette puller (Sutter Instrument, Novato, CA 94949, USA). The pipettes with tip diameters of 50 to 100 μm (recording bandwidth of >30 kHz) were filled with artificial perilymph. Signals were amplified with a recording bandwidth of dc (100 kHz) using a laboratory designed and constructed preamplifier (J. Hartley). With low-impedance electrodes, CM was measured at levels of 20 dB SPL in response to 5-kHz tones in mice with DPOAEs (see below) that were sensitive throughout the 1- to 70-kHz range of the sound system. CAP tuning curves were derived from simultaneous tone-on-tone masking (*24*) using a 10-ms probe tone centered on a 40-ms masker tone. The probe tone was set to a level where a stable CAP appeared just above the recording noise floor. The frequency of the masker was set, and its attenuation was adjusted until the probe tone CAP was suppressed. The masker frequency and level were noted; a new masker frequency was set, and the process was repeated.

Sound was delivered via a probe with its tip within 1 mm of the tympanic membrane and coupled to a closed acoustic system comprising two Microtech Gefell GmbH 1-inch MK102 microphones for delivering tones and a Brüel & Kjær (www.Bksv.co.uk) 3135 0.25-inch microphone for monitoring sound pressure at the tympanum and DPOAEs. Spontaneous emissions were measured using a Knowles FG-23652 microphone (Knowles Electronics LLC., Itasca, IL) and a laboratory-built amplifier (J. Hartley). The sound system was calibrated in situ for frequencies between 1 and 70 kHz, and known SPLs were expressed in dB SPL with reference to 2×10^{-5} Pa. Tone pulses with rise/fall times of 1 ms were synthesized by a Data Translation 3010 (Data Translation, Marlboro, MA) data acquisition board, attenuated, and used for sound system calibration and the measurement of electrical and acoustical cochlear responses. To measure DPOAEs, primary tones were set to generate 2f1 − f2 distortion products at frequencies between 1 and 50 kHz. DPOAEs were measured for f1 levels from 10 to 80 dB SPL, with the levels of the f2 tone set 10 dB below that of the f1 tone. DPOAE threshold curves represented the level of the f2 tone that produced a 2f1 − f2 DPOAE with a level of 0 dB SPL where the f2:f1 frequency ratio was 1.23. System distortion during DPOAE measurements was 80 dB below the primary tone levels.

Tone-evoked BM displacements were measured by focusing the beam of a self-mixing, laser-diode interferometer (*21*) through the round window membrane to form a 20-μm spot on the center of the BM in the 50- to 56-kHz region of the cochlea. The interferometer was calibrated at each measurement location by vibrating the piezo stack on which it was mounted over a known range of displacements. At the beginning of each set of BM measurements, it was ensured that the 0.2-nm threshold used as the criterion for threshold was at least as sensitive as the 0–dB SPL threshold for the DPOAEs before the cochlea was exposed. BM measurements were checked continuously for changes in the sensitivity of the measurement (because of changes in alignment or fluid on the round window) and in the condition of the preparation. If thresholds of the latter were changed by more than 5 to 10 dB SPL, the measurements were terminated. Tone pulses with rise/fall times of 1 ms were used for BM measurements. Stimulus delivery to the sound system and interferometer for calibration and processing of signals from the microphone amplifiers, microelectrode recording amplifiers, and interferometer were controlled by a DT3010/32 (Data Translation, Marlboro, MA) board by a PC running MATLAB (MathWorks, Natick, MA) at a sampling rate of 250 kHz. The output signal of the interferometer was processed using a digital phase-locking algorithm, and instantaneous amplitude and phase of the wave were recorded.

Measurements were made without knowledge of genotype. Phenotypic differences between +/+ and *Emilin2*$^{-/-}$ mice were strong (and could reliably predict genotype). Less than 5% of all measurements were terminated because the physiological state of the preparation changed during measurement; in which case, data from the sample were excluded.

Auditory-evoked brainstem response

The auditory-evoked brainstem response was measured using a SmartEP system (Intelligent Hearing Systems) in a sound-attenuated chamber, as described in (*46*). Mice at ~3 months of age were anesthetized with Avertin (0.25 mg/g body weight). The duration of testing was about 20 min, and the mouse then recovered from anesthesia under a warming lamp. Student's *t* test was used to assess statistical significance of pairwise comparisons between genotypes.

Experimental design and statistical analyses

The *Emilin2* lacZ knock-in was designed to allow tracking of expression of the gene in heterozygotes and functional analysis of the

deletion of emilin 2 in homozygotes. *Emilin2*$^{+/-}$ mice were crossed to generate +/+, +/−, and −/− genotypes. Male and female mice were studied in approximately equal proportions. No phenotypic differences were observed between males and females. Physiological tests were performed on +/+ and −/− littermates to minimize variations of age, environment, or genetic background. Tests were performed on 3- to 5-week-old mice to reduce the possibility of progressive loss of high-frequency responses, which is common in many mouse strains. Tests were performed on all mice in a litter without knowledge of genotype. Randomization was not appropriate because we had no foreknowledge of the genotype. Genotypes were determined after an experiment. For statistical analysis of physiological experiments, data were compared for at least five +/+ and five *Emilin2*$^{-/-}$ mice, obtained from recordings of two or three complete litters. For analysis of BM tuning curves, 15 +/+ and 15 −/− mice in total were tested. For neural masking frequency tuning curves and DPOAE analyses, groups of five mice were tested. Data were plotted as means ± SD using FigP (www.figpsoft.com) or Origin (www.originlab.com) software. Statistical tests were performed with GraphPad Prism (www.graphpad.com/quickcalcs), and comparisons were made using unpaired *t* tests for unequal variances unless otherwise noted. *P* values are noted as absolute values with *t* values and df. For consistent differences between two genotypes over a range of frequencies, *P* values are noted as $P < 0.005$, $P < 0.001$, and $P < 0.0001$ in Figs. 5 and 6, for clarity of presentation. Morphological and cell count data were obtained on histological sections from groups of six mice at ~1 month of age (for consistency with physiological analyses at a similar age) and adult ages. Comparisons of +/+ and −/− groups were analyzed by unpaired *t* tests using GraphPad Prism 8.1.

Software and code

For physiological recordings, data acquisition and data analysis were performed using a PC with programs written in MATLAB (MathWorks, MA). The programs are available upon request from authors A.N.L. and I.J.R. Please note that the programs were written to communicate with specific hardware (Data Translation 3010 board and custom-made GPIB-controlled attenuators) and will need modifications to be used with different hardware. Birefringent optical images were analyzed using OpenPolScope software (www.openpolscope.org), which included Micro-Manager version 1.4.22 and OpenPolScope version 3.2, with further analysis using Fiji, Photoshop (Adobe), and Origin software (MicroCal LLC). Confocal fluorescent images were processed using Photoshop (Adobe) and ImageJ (https://imagej.nih.gov/ij/).

SUPPLEMENTARY MATERIALS

Supplementary material for this article is available at http://advances.sciencemag.org/cgi/content/full/6/24/eaba2634/DC1

View/request a protocol for this paper from *Bio-protocol*.

REFERENCES AND NOTES

1. G. von Békésy, *Experiments in Hearing* (McGraw-Hill, 1960).
2. R. Fettiplace, Hair cell transduction, tuning, and synaptic transmission in the mammalian cochlea. *Compr. Physiol.* **7**, 1197–1227 (2017).
3. C. J. Sumner, T. T. Wells, C. Bergevin, J. Sollini, H. A. Kreft, A. R. Palmer, A. J. Oxenham, C. A. Shera, Mammalian behavior and physiology converge to confirm sharper cochlear tuning in humans. *Proc. Natl. Acad. Sci. U.S.A.* **115**, 11322–11326 (2018).
4. L. M. Cabezudo, The ultrastructure of the basilar membrane in the cat. *Otolaryngology* **86**, ORL-433 (1978).
5. S. Iurato, Submicroscopic structure of the membranous labyrinth. III. The supporting structure of Corti's organ (basilar membrane, limbus spiralis and spiral ligament). *Z. Zellforsch. Mikrosk. Anat.* **56**, 40–96 (1962).
6. F. J. Dreiling, M. M. Henson, O. W. Henson Jr., The presence and arrangement of type II collagen in the basilar membrane. *Hear. Res.* **166**, 166–180 (2002).
7. S. Echteler, R. Fay, A. Popper, Structure of the mammalian cochlea, in *Comparative Hearing: Mammals*, R. Fay, A. Popper, Eds. (Springer, 1994), pp. 134–171.
8. W. Kolmer, Studien am Labyrinth von Insectivoren. Sitzungsberichte der Kaiserlichen Akademie der Wissenschaften (in Wien). *Mathematisch-Naturwissenschaftliche Klasse* **122**, 29–52 (1913).
9. S. Kapuria, C. R. Steele, S. Puria, Unraveling the mystery of hearing in gerbil and other rodents with an arch-beam model of the basilar membrane. *Sci. Rep.* **7**, 228 (2017).
10. P. A. Santi, J. T. Larson, L. T. Furcht, T. S. Economou, Immunohistochemical localization of fibronectin in the chinchilla cochlea. *Hear. Res.* **39**, 91–101 (1989).
11. P. D. Munyer, B. A. Schulte, Immunohistochemical localization of keratan sulfate and chondroitin 4- and 6- sulfate proteoglycans in subregions of the tectorial and basilar membranes. *Hear. Res.* **79**, 83–93 (1994).
12. L. L. Amma, R. Goodyear, J. S. Faris, I. Jones, L. Ng, G. Richardson, D. Forrest, An emilin family extracellular matrix protein identified in the cochlear basilar membrane. *Mol. Cell. Neurosci.* **23**, 460–472 (2003).
13. A. Schiavinato, D. R. Keene, A. P. Wohl, D. Corallo, A. Colombatti, R. Wagener, M. Paulsson, P. Bonaldo, G. Sengle, Targeting of EMILIN-1 and EMILIN-2 to fibrillin microfibrils facilitates their incorporation into the extracellular matrix. *J. Invest. Dermatol.* **136**, 1150–1160 (2016).
14. A. Colombatti, P. Spessotto, R. Doliana, M. Mongiat, G. M. Bressan, G. Esposito, The EMILIN/multimerin family. *Front. Immunol.* **2**, 93 (2011).
15. A. Paulitti, E. Andreuzzi, D. Bizzotto, R. Pellicani, G. Tarticchio, S. Marastoni, C. Pastrello, I. Jurisica, G. Ligresti, F. Bucciotti, R. Doliana, R. Colladel, P. Braghetta, E. Poletto, A. Di Silvestre, G. Bressan, A. Colombatti, P. Bonaldo, M. Mongiat, The ablation of the matricellular protein EMILIN2 causes defective vascularization due to impaired EGFR-dependent IL-8 production affecting tumor growth. *Oncogene* **37**, 3399–3414 (2018).
16. M. Huang, D. Sannaningaiah, N. Zhao, Y. Gong, J. Grondolsky, J. Hoover-Plow, EMILIN2 regulates platelet activation, thrombus formation, and clot retraction. *PLOS ONE* **10**, e0115284 (2015).
17. A. Axelsson, Comparative anatomy of cochlear blood vessels. *Am. J. Otolaryngol.* **9**, 278–290 (1988).
18. W. Liu, F. Atturo, R. Aldaya, P. Santi, S. Cureoglu, S. Obwegeser, R. Glueckert, K. Pfaller, A. Schrott-Fischer, H. Rask-Andersen, Macromolecular organization and fine structure of the human basilar membrane - relevance for cochlear implantation. *Cell Tissue Res.* **360**, 245–262 (2015).
19. W. M. Petroll, Differential interference contrast and confocal reflectance imaging of collagen organization in three-dimensional matrices. *Scanning* **28**, 305–310 (2006).
20. R. Oldenbourg, Polarized light field microscopy: An analytical method using a microlens array to simultaneously capture both conoscopic and orthoscopic views of birefringent objects. *J. Microsc.* **231**, 419–432 (2008).
21. A. N. Lukashkin, M. E. Bashtanov, I. J. Russell, A self-mixing laser-diode interferometer for measuring basilar membrane vibrations without opening the cochlea. *J. Neurosci. Methods* **148**, 122–129 (2005).
22. I. J. Russell, P. K. Legan, V. A. Lukashkina, A. N. Lukashkin, R. J. Goodyear, G. P. Richardson, Sharpened cochlear tuning in a mouse with a genetically modified tectorial membrane. *Nat. Neurosci.* **10**, 215–223 (2007).
23. M. Müller, K. von Hünerbein, S. Hoidis, J. W. Smolders, A physiological place–frequency map of the cochlea in the CBA/J mouse. *Hear. Res.* **202**, 63–73 (2005).
24. P. Dallos, M. A. Cheatham, Compound action potential (AP) tuning curves. *J. Acoust. Soc. Am.* **59**, 591–597 (1976).
25. A. N. Lukashkin, I. J. Russell, Analysis of the f_2–f_1 and $2f_1$–f_2 distortion components generated by the hair cell mechanoelectrical transducer: Dependence on the amplitudes of the primaries and feedback gain. *J. Acoust. Soc. Am.* **106**, 2661–2668 (1999).
26. C. A. Shera, Mechanisms of mammalian otoacoustic emission and their implications for the clinical utility of otoacoustic emissions. *Ear Hear.* **25**, 86–97 (2004).
27. M. A. Cheatham, Y. Zhou, R. J. Goodyear, P. Dallos, G. P. Richardson, Spontaneous otoacoustic emissions in *Tecta*$^{Y1870C/+}$ mice reflect changes in cochlear amplification and how it is controlled by the tectorial membrane. *eNeuro* **5**, ENEURO.0314-18.2018, (2018).
28. J. B. Allen, M. M. Sondhi, Cochlear macromechanics: Time domain solutions. *J. Acoust. Soc. Am.* **66**, 123–132 (1979).
29. J. Meaud, K. Grosh, The effect of tectorial membrane and basilar membrane longitudinal coupling in cochlear mechanics. *J. Acoust. Soc. Am.* **127**, 1411–1421 (2010).

30. L. Robles, M. A. Ruggero, Mechanics of the mammalian cochlea. *Physiol. Rev.* **81**, 1305–1352 (2001).
31. C. A. Shera, The spiral staircase: Tonotopic microstructure and cochlear tuning. *J. Neurosci.* **35**, 4683–4690 (2015).
32. D. T. Kemp, A. M. Brown, An integrated view fo cochlear mechanical nonlinearities observable form the ear canal, in *Mechanics of Hearing,* E. de Boer, M. A. Viergever, Eds. (Springer, 1983), pp. 75–82.
33. G. W. S. Burwood, I. J. Russell, A. N. Lukashkin, Rippling pattern of distortion product otoacoustic emissions evoked by high-frequency primaries in guinea pigs. *J. Acoust. Soc. Am.* **142**, 855–862 (2017).
34. L. J. Stover, S. T. Neely, M. P. Gorga, Latency and multiple sources of distortion product otoacoustic emissions. *J. Acoust. Soc. Am.* **99**, 1016–1024 (1996).
35. D. T. Kemp, Stimulated acoustic emissions from within the human auditory system. *J. Acoust. Soc. Am.* **64**, 1386–1391 (1978).
36. A. N. Lukashkin, M. N. Walling, I. J. Russell, Power amplification in the mammalian cochlea. *Curr. Biol.* **17**, 1340–1344 (2007).
37. J. Meaud, K. Grosh, Effect of the attachment of the tectorial membrane on cochlear micromechanics and two-tone suppression. *Biophys. J.* **106**, 1398–1405 (2014).
38. W. He, D. Kemp, T. Ren, Timing of the reticular lamina and basilar membrane vibration in living gerbil cochleae. *eLife* **7**, e37625 (2018).
39. P. M. Sellick, I. J. Russell, Two-tone suppression in cochlear hair cells. *Hear. Res.* **1**, 227–236 (1979).
40. P. Dallos, M. C. Billone, J. D. Durrant, C. Wang, S. Raynor, Cochlear inner and outer hair cells: Functional differences. *Science* **177**, 356–358 (1972).
41. I. J. Russell, P. M. Sellick, Intracellular studies of hair cells in the mammalian cochlea. *J. Physiol.* **284**, 261–290 (1978).
42. I. J. Russell, M. Kössl, Micromechanical responses to tones in the auditory fovea of the greater mustached bat's cochlea. *J. Neurophysiol.* **82**, 676–686 (1999).
43. G. Nieuweiler, *The Biology of Bats: Echolocation* (Oxford Univ. Press, 2000), chap. 6.
44. L. Ng, M. W. Kelley, D. Forrest, Making sense with thyroid hormone—The role of T_3 in auditory development. *Nat. Rev. Endocrinol.* **9**, 296–307 (2013).
45. Q. Y. Zheng, K. R. Johnson, L. C. Erway, Assessment of hearing in 80 inbred strains of mice by ABR threshold analyses. *Hear. Res.* **130**, 94–107 (1999).
46. L. Ng, A. Hernandez, W. He, T. Ren, M. Srinivas, M. Ma, V. A. Galton, D. L. S. Germain, D. Forrest, A protective role for type 3 deiodinase, a thyroid hormone-inactivating enzyme, in cochlear development and auditory function. *Endocrinology* **150**, 1952–1960 (2009).

Acknowledgments: We thank T. Tani, M. Koike Tani, and R. Oldenburg at the MBL, Woods Hole, MA for providing facilities and training for optical imaging. **Funding:** This work was supported by the intramural research program at NIDDK at the NIH (Y.-W.C., L.N., and D.F.). Work at the University of Brighton was funded by the Medical Research Council MR/N004299/1 grant. **Author contributions:** I.J.R., D.F., L.N., and A.N.L. designed the research. S.L. performed and analyzed polarized light microscopy measurements. A.N.L. wrote computer programs. V.A.L. and I.J.R. performed and analyzed physiological recordings. L.N. and Y.-W.C. performed molecular and anatomical analyses. D.F. and I.J.R. wrote the paper with input from the other authors. **Competing interests:** The authors declare that they have no competing interests. **Data and materials availability:** All data needed to evaluate the conclusions in the paper are present in the paper and/or the Supplementary Materials. Additional data related to this paper may be requested from the authors.

Submitted 19 November 2019
Accepted 2 April 2020
Published 10 June 2020
10.1126/sciadv.aba2634

Citation: I. J. Russell, V. A. Lukashkina, S. Levic, Y.-W. Cho, A. N. Lukashkin, L. Ng, D. Forrest, Emilin 2 promotes the mechanical gradient of the cochlear basilar membrane and resolution of frequencies in sound. *Sci. Adv.* **6**, eaba2634 (2020).

Science Advances

Emilin 2 promotes the mechanical gradient of the cochlear basilar membrane and resolution of frequencies in sound

Ian J. Russell, Victoria A. Lukashkina, Snezana Levic, Young-Wook Cho, Andrei N. Lukashkin, Lily Ng and Douglas Forrest

Sci Adv **6** (24), eaba2634.
DOI: 10.1126/sciadv.aba2634

Science Advances (ISSN 2375-2548) is published by the American Association for the Advancement of Science, 1200 New York Avenue NW, Washington, DC 20005. The title *Science Advances* is a registered trademark of AAAS.